Nuclear Materials and Energy 9 (2016) 604–609

Contents lists available at ScienceDirect

Nuclear Materials and Energy

journal homepage: www.elsevier.com/locate/nme

Improved ERO modelling for spectroscopy of physically and chemically assisted eroded beryllium from the JET-ILW☆

D. Borodin[a,*], S. Brezinsek[a], I. Borodkina[b,a], J. Romazanov[a], D. Matveev[a], A. Kirschner[a], A. Lasa[c], K. Nordlund[d], C. Björkas[d], M. Airila[d], J. Miettunen[e], M. Groth[e], M. Firdaouss[f], JET Contributors[1]

[a] Forschungszentrum Jülich GmbH, Institut für Energie- und Klimaforschung - Plasmaphysik, 52425 Jülich, Germany
[b] National Research Nuclear University MEPhI, 31, Kashirskoe sh., 115409, Moscow, RF
[c] Oak Ridge National Laboratory, Oak Ridge, TN 37831-6169, USA
[d] VTT Technical Research Centre of Finland, P.O.Box 1000, FIN-02044 VTT, Finland
[e] Aalto University, P.O.Box 14100, FIN-00076 Aalto, Finland
[f] CEA, IRFM, F-13108 St Paul-Lez-Durance, France

ARTICLE INFO

Article history:
Available online 18 October 2016

Keywords:
Beryllium
Erosion
JET ITER-like wall
Spectroscopy

ABSTRACT

Physical and chemical assisted physical sputtering were characterised by the Be I and Be II line and BeD band emission in the observation chord measuring the sightline integrated emission in front of the inner beryllium limiter at the torus midplane. The 3D local transport and plasma-surface interaction Monte-Carlo modelling (ERO code [18]) is a key for the interpretation of the observations in the vicinity of the shaped solid Be limiter. The plasma parameter variation (density scan) in limiter regime has provided a useful material for the simulation benchmark. The improved background plasma parameters input, the new analytical expression for particle tracking in the sheath region and implementation of the BeD release into ERO has helped to clarify some deviations between modelling and experiments encountered in the previous studies [4,5]. Reproducing the observations provides additional confidence in our 'ERO-min' fit for the physical sputtering yields for the plasma-wetted areas based on simulated data.

Introduction

Estimating beryllium (Be) sputtering by plasma ions is a key issue for ITER as erosion determines the life time of plasma-facing components [1,2] and impacts on the tritium retention by co-deposition with Be, which must be kept within the nuclear safety limit of ITER. The first experimental campaign at JET equipped with the ITER-Like Wall (ILW) [3], with Be limiters and W divertor, included several experiments dedicated to the determination of first wall erosion. In the present paper we focus on three solid Be components ('tiles') of the poloidal guard limiter (GL) positioned at the inner wall (IW) close to the midplane. The limiter plasmas shifted towards the IW were used to have a single interaction point useful for the determination of Be yields. The magnetic configuration and plasma current was kept unchanged, just the D fuelling was varied leading to the respective increase of electronic density with an opposite effect for its temperature and corresponding impact energy of sputtering ions. Passive spectroscopy of Be atoms, Be ions and BeD molecules were used for the characterization of erosion and its contributors. This work is a continuation and significant update of previous studies [4,5].

3D local transport modelling of eroded Be has been shown previously to be absolutely essential for the interpretation of sightline-integrated spectroscopy [6]. Similar to previous studies we utilize the Monte-Carlo (MC) code ERO for this purpose. The code applies physical sputtering data based on molecular dynamics (MD) [7] and binary-collision approximation calculations [8]. This data is being benchmarked by comparison of the ERO synthetic results with the experimental observations. It should be mentioned that a very similar work goes in parallel for the OW of JET [9].

☆ EUROfusion Consortium, JET, Culham Science Centre, Abingdon, OX14 3DB, UK.

* Corresponding author.
E-mail address: d.borodin@fz-juelich.de (D. Borodin).

[1] See Appendix of F. Romanelli et al., 25th IAEA Fusion Energy Conference (2014, St. Petersburg, Russia)

http://dx.doi.org/10.1016/j.nme.2016.08.013

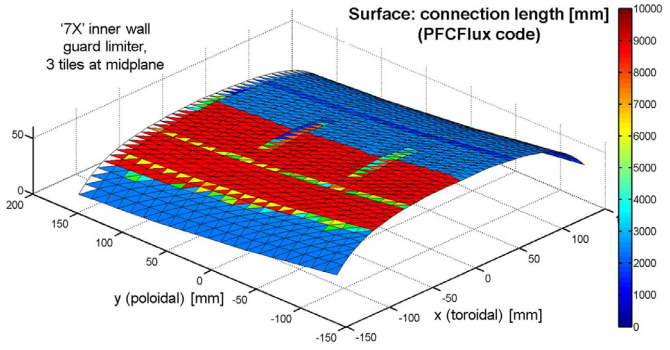

Fig. 1. The connection lengths simulated by the PFCFlux code [12] along the IWGL limiter surface part (3 tiles) included into the ERO simulation volume.

A number of improvements have been carried out in comparison to the previous studies. The background plasma (ERO input) was revised including plasma conditions deduced from embedded Langmuir probes [10]. Moreover, the analytical expressions for the electric field in the sheath and for the very last part of the particle trajectory just before the ion collision with the surface were incorporated [11] providing more precise distributions of ion energies and angles with the surface on deuteron (D) impact. This affects the effective sputtering yield at each point of PFC surface with varying local B-field angle with it and local plasma temperature. The influence of the initial metastable population [12] after the physical sputtering on the light emission is studied. The contributions of self-sputtering and chemically assisted physical sputtering [7] are assessed and discussed.

The inclusion of the above mentioned effects shall reduce uncertainties and give further confidence in the models and underlying data, including the fit used for the Be sputtering yields.

Passive spectroscopy and 3D local transport simulation

Particles eroded from PFCs, including the IWGL considered in the present paper, are released into the plasma, dissociated (for molecules), and ionized or excited at a certain distance from the surface. The penetration depth is determined mostly by the ionization rates, plasma parameter distribution, initial direction and velocity of eroded particles. The erosion by the background plasma is calculated as multiplication of the D and Be impurity fluxes by respective effective yields (see below) for physical sputtering. For the D-flux additionally the chemically assisted release of BeD is considered. Be ions are being trapped by the magnetic field and driven by the plasma flow and electric field. These effects are easy to describe in a deterministic way. However, the ions also experience stochastic processes, for instance, further ionization or anomalous transport often treated like cross-field diffusion. The 3D MC simulations of the mentioned processes are proved to be an efficient way to obtain the resulting species density and light emission plumes. The ERO code follows a representative amount of MC test particles on their way through the plasma, calculates their spectroscopic light emission (for the lines or molecular bands of interest, mostly the ones observed in the experiment) and integrates it within the observation chord of the diagnostics.

It should be noted that the surface of the IWGL is only partially plasma-wetted due to shadowing of neighbored limiters toroidally separated from the observed one included in the simulations by the field tracing PFCFlux code [13] which contains the detailed ILW geometry (Fig. 1). In a first approximation it is possible to assume that the erosion in the shadowed areas is negligible. In such an approach variations along the limiter surface between connection lengths below the certain value characteristic for the limiter ridge is neglected. However, later on, this approach can be refined following the procedure carried out in [14].

In Fig. 2 the side views of the ERO simulated emission patterns are shown. The cylindrical sightline (in fact conical, however the

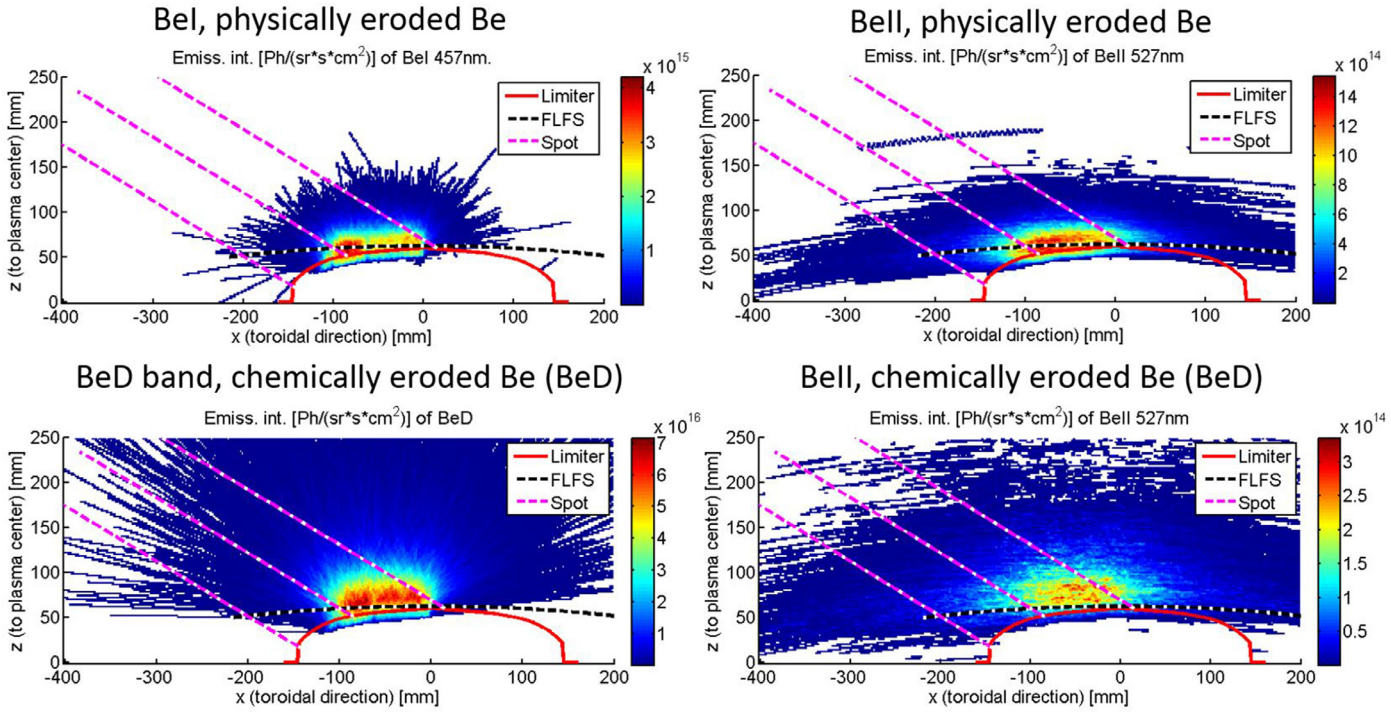

Fig. 2. Be I and Be II light emission in the close to the solid Be shaped IW limiter. ERO simulations for Be sputtered from the wall physically alongside with the simulations for chemically released BeD. Be II plume is determined by the shadowing local transport and ionization/dissociation.

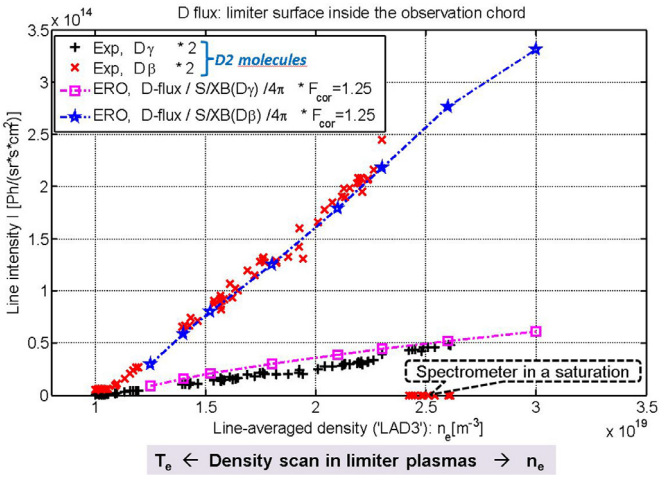

Fig. 3. D spectroscopy (Balmer-α and Balmer-β) characterizing the plasma ion flux to the surface. Experimental results are multiplied by 2 to account for the mostly molecular D release as D_2 which dissociates preferably through the channel with ionization of one of the atoms; this way every second released D atom is lost for the observation.

difference for the small fraction inside the simulation volume is negligible) projection is labeled in the Figure; its impact angle with the limiter is also indicated. The observation geometry affects the fraction of the emission entering the volume of integration. This fraction varies with distance of the plasma with the limiter due to changing plasma parameters, species ionization state and MS population. As it can be seen in Fig. 2, the emission pattern for the BeD band varies from the one for Be I line emission due to the larger penetration depth of the molecules. Both are also essentially different for the Be ions which are produced by dissociation of molecules and associated ionization, as well as directly ionized after physical sputtering.

Improved plasma parameters

As can be inferred from the preceding section, ERO results are very dependent on the local 3D distribution of plasma parameters. For the current studies they are reconstructed from the experimental data (effective radius profiles), in 2D, for a poloidal cross-section, applying the 2-point (onion skin) model [5]. Moreover, toroidal symmetry is assumed to translate the data into the 3D simulation box around the Be limiter. The new plasma parameter set was developed using the data from the embedded probes and re-interpreted spectroscopy. The revised electron temperature in the plasma background is about a factor 2 smaller than previously used (T_e~15 eV at the separatrix). In addition, the D-flux during the plasma density scan was enforced to follow the experimental ramp characterized by D_γ spectroscopy measuring the recycling flux at the limiter (Fig. 3). The figure shows that the revised plasma background reproduces well the D_β/ D_γ ratio and a very satisfactory simulation of the absolute values in the observation chord (sightline).

Another test for the plasma parameters and atomic data used [15] are the Be II line ratios (Fig. 4) used earlier in [6] for T_e determination. All 3 line ratios are reproduced well. The Be II level system does not contain significant metastables, thus the behaviour of the line ratios is determined by the photon-emission coefficients presented on the right hand side of Fig. 4. Though the ratios indicate that the assumed T_e is slightly insufficient, the deviations (~20%) are well within the measurement uncertainties. It should be noted that in Fig. 4 the ratios for physically eroded particles are presented. The fraction released as BeD penetrates deeper into the plasma due to the dissociation and subsequent ionization and emits light at large T_e, so it can only reduce the ratio deviations.

A last interesting parameter for a benchmark is the branching ratio between BeD dissociative ionization to BeD^+ and dissociation to Be neutrals deduced from the line intensity drops during the surface temperature scan in [6]. It was shown that only 25% of the molecules are going through the channel $BeD + e \rightarrow BeD^+ + e + e'$.

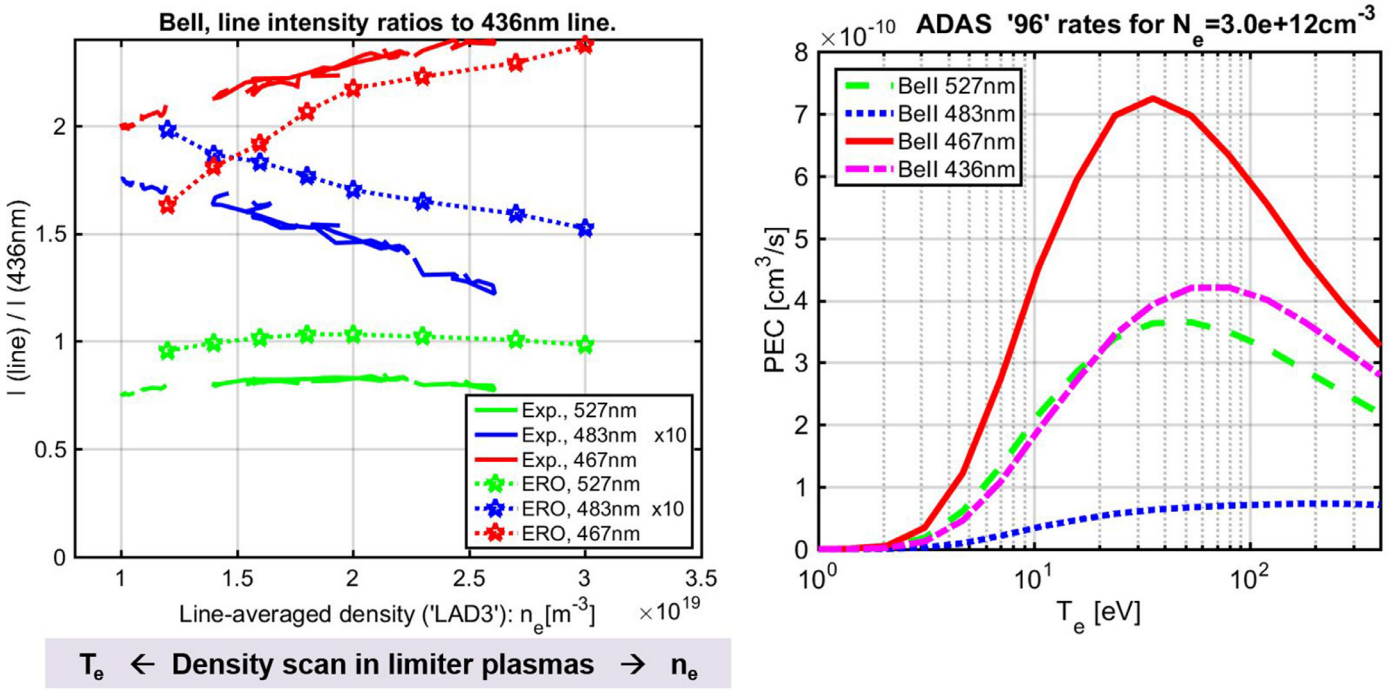

Fig. 4. Line ratios in Be II sputtered from the IW GL (left) and the relevant photon efficient coefficients from ADAS (right) [14].

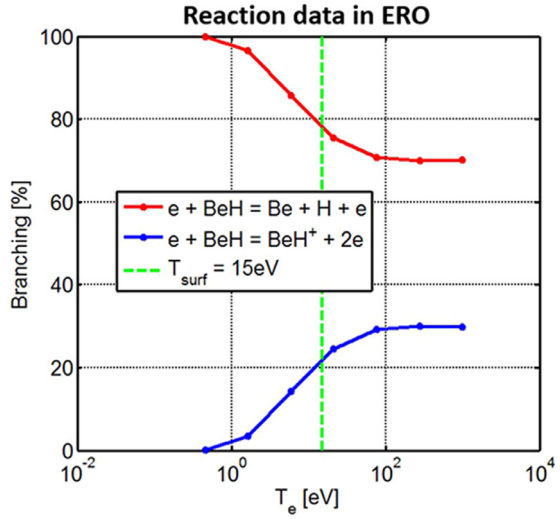

Fig. 5. Branching rates for the BeD decay reactions contained in ERO databank [15]. At marked $T_e = 15$ eV the fractions are really close to the observed [6] 75%:25% values.

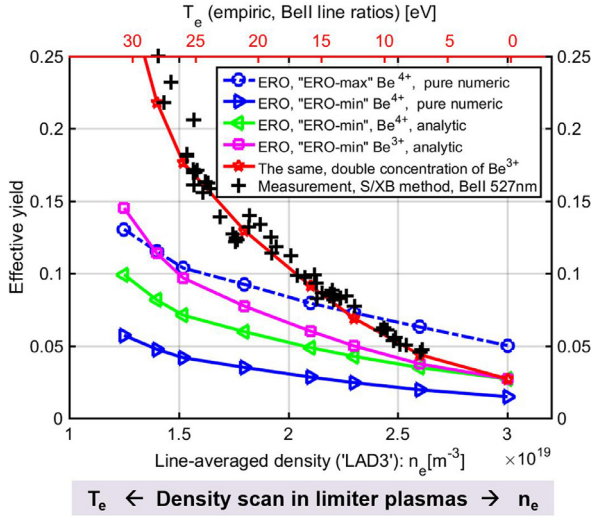

Fig. 6. The effective sputtering yields in ERO and S/XB method measurements [6] (using Be II 527nm line). The influence of the physical sputtering fits for pure Be ('ERO-max') and Be with 50%D in the interaction layer ('ERO-min') [3]. The influence of the recently implemented analytical expressions [10] is shown ('analytic') as well as influence of the intrinsic Be impurity concentration and respective self-sputtering.

The rates for these reactions have already been implemented in ERO [16]. The branching ratio obtained from these data comes really close to the experimental observations in particular at $T_e = 15$ eV (Fig. 5). As mentioned earlier, this is the corrected value at the separatrix. The limiter ridge stays about 2 cm inwards the scrape-off-layer. As most penetration depths in the modelled experiment are about few cm, most light emission and dissociation should happen close by.

Effective sputtering yields benchmark

As it was shown in [5], the ion impact angle $\boldsymbol{\alpha_{imp}}$ and energy $\boldsymbol{E_{imp}}$ distributions are of importance for physical sputtering in case of the shallow angle between the PFC surface and the magnetic field. Therefore we have to calculate the effective values for each surface location, which are proved to vary with the B-field angle to the surface normal $\boldsymbol{\eta}$ and local $\boldsymbol{T_e}$. In Fig. 6 the effective yields $\boldsymbol{Y^{Eff}(\eta, T_e)}$ integrated from the basic fits $\boldsymbol{Y(E_{imp}, \alpha_{imp})}$ e.g. 'ERO-min', with the $(\boldsymbol{E_{imp}}, \boldsymbol{\alpha_{imp}})$ distributions on impact are depicted. These distributions are generated:

(a) numerically, as formerly done, by a special ERO preliminary run [5];
(b) by the new analytical expressions for the E-field and ion velocity in the sheath [11].

The $\boldsymbol{Y^{Eff}}$ vary along the limiter surface, however the values are averaged by ERO along the whole sightline-relevant erosion zone excluding the shadowed area.

The reliability of the analytical expressions have been proved [11] by a very good agreement with particle-in-cell (PIC) simulations. The only advantage remaining yet on the numeric ERO approach (the direct incorporation of the analytical solution in ERO is ongoing) is that it tracks the sputtering ions right from the stagnation point, thus takes into account their thermalization in the plasma. The analytical approach starts for now with a reasonable ion velocity distribution at the sheath entrance as initial condition. It leads to broader angle and energy distributions than the ones simulated by ERO. This, in particular the $\boldsymbol{\alpha_{imp}}$ distribution, results in an increase of the resulting effective yields of ~30% for 'ERO-min' (Fig. 6). From the technical side, the analytical approach suits better for that task as the numeric approach suffers due to the necessity to decrease the simulation step in the rising sheath E-field down to 10^{-13}–10^{-15} s to produce the accurate angles on impact.

Fig. 6 demonstrates the influence of the self-sputtering by the intrinsic Be impurity in the plasma contributing to the total erosion yield proportionally to its concentration f_{Be}:

$$\boldsymbol{Y_{total} = Y^{Eff}_{Be\leftarrow D}(1-f_{Be}) + Y^{Eff}_{Be\leftarrow Be}(f_{Be})}, \quad (1)$$

where $\boldsymbol{Y^{Eff}_{Be\leftarrow D}}$ and $\boldsymbol{Y^{Eff}_{Be\leftarrow Be}}$ are the effective sputtering yields for D and Be ('self-sputter') eroding species. Similar to the previous studies we deduce f_{Be} from the measured effective charge Z_{eff}. Be impurity comes partially from the closest PFCs, but also from the core as Be^{4+} ($\boldsymbol{Z_{Be}=4}$), which however can also recombine e.g. to Be^{3+} on its way. Self-consistent modelling would demand including a much larger volume, with all relevant impurity sinks and sources and self-consistent tracking of Be ions. For now we can just assume that all Be ions come for instance as Be^{4+} or alternatively Be^{3+}. The charge $\boldsymbol{Z_{Be}}$ has no influence on the sputtering yield by itself, however it affects the charge-dependent acceleration in the sheath, though the yield dependence on energy is stagnating. Thus the erosion upon assumption of 3+ charge is larger due to the amount of atoms deduced from Z_{eff} (Fig. 6) matching better with the experiment.

The standard JET Z_{eff} diagnostics has no radial resolution, whereas it is to expect that the impurity content at the radial positions corresponding to the most effective erosion locations at the limiter ridge, is larger. It can be seen in Fig. 6 that the assumption of $\boldsymbol{Z_{Be}}$=3 charge and double concentration at the erosion location leads to a perfect match with the experiment. This is of course more an indication than a proof that we interpret the self-sputtering correctly. On the right side of the plots corresponding to large plasma densities and low temperatures (low energies of sputtering ions) the effect of self-sputtering goes to zero as the measured Z_{eff}~1. In this region the calculated curves assuming 'ERO-min' with analytic distributions are matching really well the experimental values obtained by the S/XB method [17] refined with the T_e adjusted according to the line ratios observed in the very same sightline [6]. On one hand, the uncertainties in intrinsic Be impurity charge and concentration do not allow to benchmark the self-sputtering yields directly, but the deviations with experiments are shown to be explainable. On the other hand, the basic data and fit for self-sputtering is produced in the same way and can be expected to be of the same accuracy. The 'ERO-max' fit on the zero

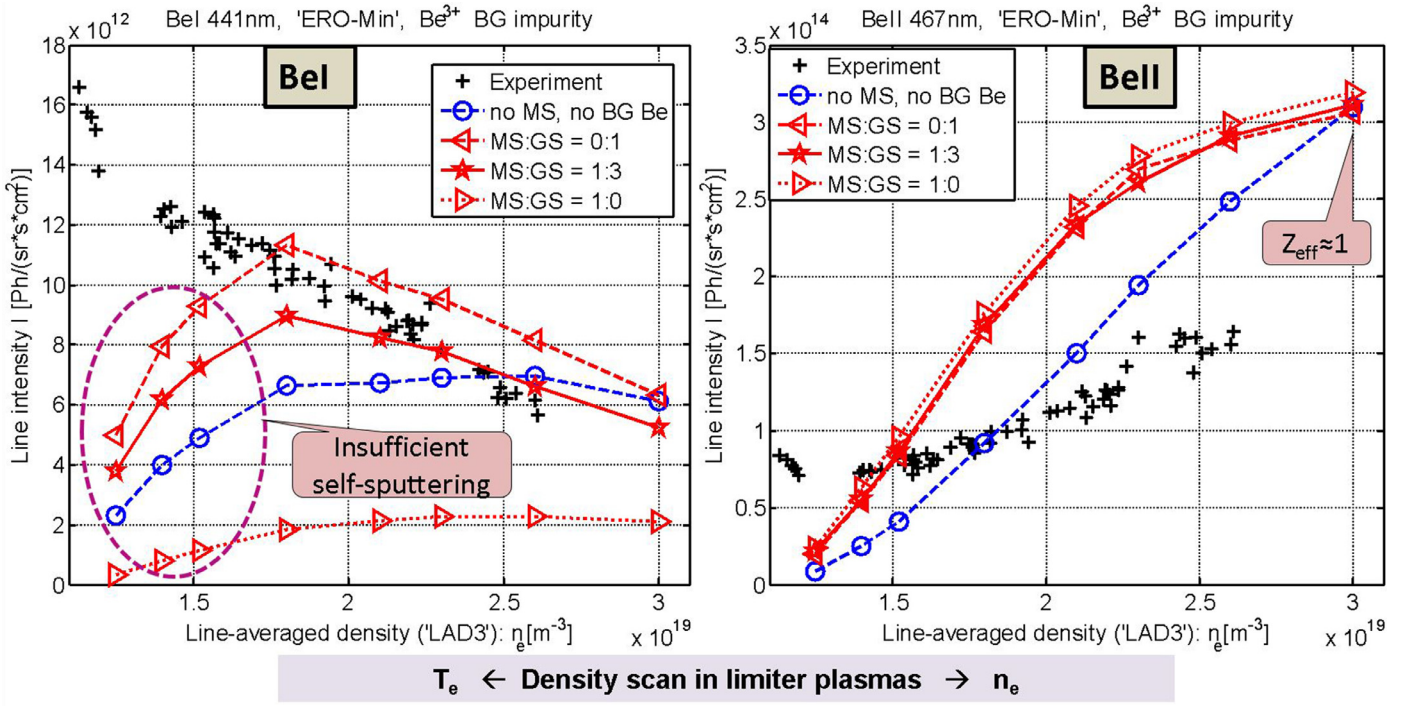

Fig. 7. ERO synthetic line intensities integrated inside the observation chord compared against the absolute experimental measurements during the density scan experiment.

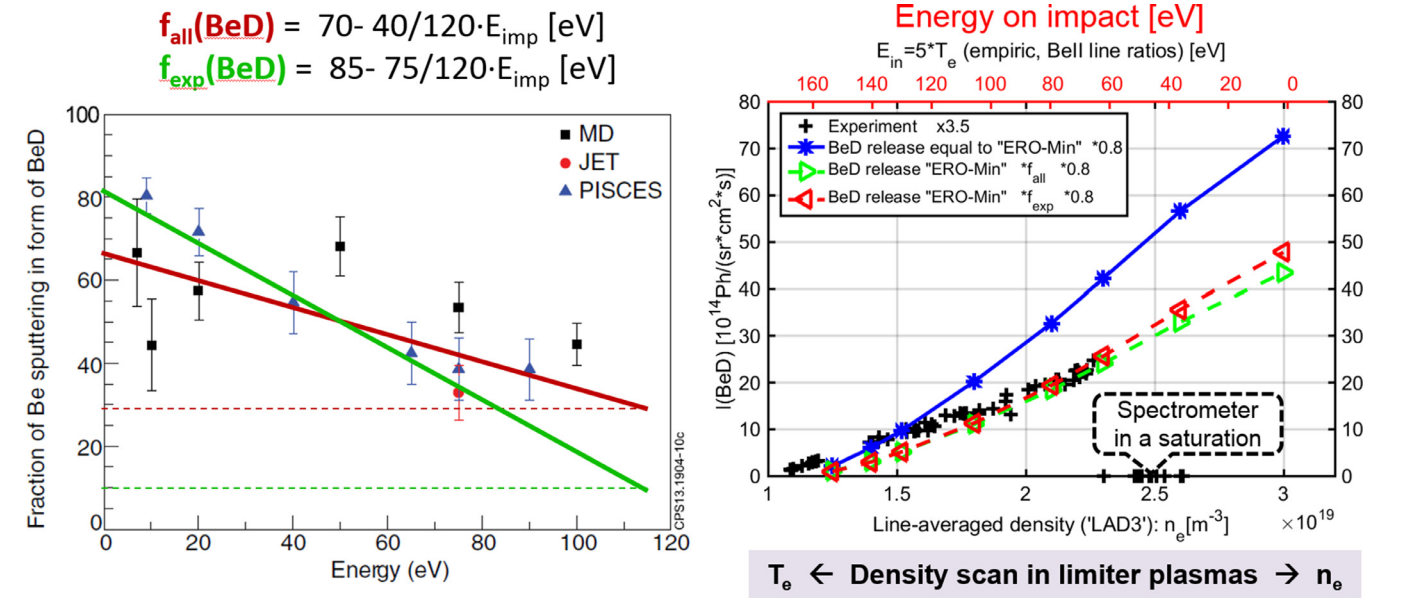

Fig. 8. The BeD band emission simulated by ERO (total) and observed in experiment (right) using the fits for the fraction of BeD release from obtained on the experimental ('PISCES', 'JET') and simulated ('MD') data from [6]. Measurements are multiplied by 3.5 to obtain the total band intensity whereas only a fraction of it depending on the vibrational and rotational temperatures is coming into the spectral window.

self-sputtering side of the curve leads to effective yields clearly larger than measured ones even if numerical impact distributions (smaller yields) are used for the integration.

A more thorough benchmark for the model and data is the direct comparison of the synthetic light in the sightline (ERO) with the experiment. Simulations involve, for instance, the spatial distribution of erosion along the PFC surface, local transport and atomic processes in the context of 3D plasma parameters (Fig. 7). An interesting effect is the initial population of the MS states in Be I just after physical sputtering (see below). It has an essential influence on the Be I line intensities. The influence of MS population on ionization to Be^+ is minimal, so the Be II lines can be used for erosion characterization. On the left of the both graphs, in the region of low density and high temperature, the self-sputtering by the Be^{3+} content in plasma deduced from Z_{eff} is insufficient similar to the respective curve on Fig. 6.

Fig. 8 shows the first attempt to reproduce the BeD A-X band (around ~500 nm) emission by ERO. The wavelength span in the experiment is limited to the band head [6], whereas the modelling considers the full electronic transition. Thus, the experimental data must be corrected by inclusion the full spectrum which can be done by spectra modelling including e.g. accounting for population

of vibrational states resulting in a correction factor of about 3.5. That means that all the synthetic results agree with experiment within 20–30% (simulated curves are multiplied by 0.8 to get the perfect match for the one based on the experimental based fit for the BeD release fraction in comparison to the 'ERO-min' physical sputtering). The linear trend is also very well reproduced.

Summary and conclusion

A significant update for modelling [5] of Be erosion at JET ILW characterized by the passive spectroscopy is carried out. The plasma parameters input was revisited by inclusion of embedded Langmuir probes information (most significant is the correction of formerly overestimated T_e). New analytical expressions were applied to generate the energy and angle sputtering ion distributions on impact determining the effective sputtering yields. At large densities ($Z_{eff} \sim 1$) the trends for both Be I and Be II lines are well reproduced. Still, the simulations overestimate the Be II light nearly by a factor of 2. Partially it can be explained by the remaining uncertainties in the plasma backgrounds and BeD data and assumptions e.g. is was supposed that BeD release does not affect physical sputtering. The BeD band intensity trend is reproduced well and the absolute value within 20%.

This benchmark increases the confidence in the results of more general and less detailed S/XB approach, which clearly indicates that 'ERO-min' fit averaged over the impact angle and energy distributions estimated using the analytical expressions from [11] can be recommended for plasma-wetted areas as the GL surface considered in this work.

The ERO modelling of BeD release, local transport and respective surface and reaction data should be further improved. For that a detailed simulation of the surface temperature scan experiment [6] would be useful. The shadowing treatment and self-sputtering assumptions should also be refined.

Acknowledgements

This work has been carried out within the framework of the EUROfusion Consortium and has received funding from the Euratom research and training programme 2014–2018 under grant agreement No 633053. The views and opinions expressed herein do not necessarily reflect those of the European Commission. Computer time on JURECA was provided by the Jülich Supercomputing Centre.

References

[1] S. Carpentier, et al., J. Nucl. Mater. 415 (2011) S165–S169.
[2] D. Borodin, et al., Phys. Scr. T145 (2011) 14008.
[3] G.F. Matthews, et al., Phys. Scr. T145 (2011) 014001.
[4] D. Borodin, et al., JNM 438 (2013) S267–S271.
[5] D. Borodin, et al., Phys. Scr. T 159 (2014) 014057.
[6] S. Brezinsek, et al., Nucl. Fusion 54 (2014) 103001.
[7] C. Björkas, et al., Plasma Phys. Control. Fusion 55 (2013) 074004.
[8] W. Eckstein, Top. Appl. Phys. 110 (2007) 33–187.
[9] C.C. Klepper, et al., Phys. Scr. T167 (2016) 014035.
[10] G. Arnoux, et al., Nucl. Fusion 53 (2013) 073016.
[11] I. Borodkina, et al., Contrib. Plasma Phys. 56 (6–8) (2016) 640–645.
[12] D. Borodin, et al., 36th EPS Conf. on Plasma Phys., 33, ECA, 2009 E, P-5.197.
[13] M. Firdaouss, et al., JNM 438 (2013) S536–S539.
[14] R. Ding, et al., Nucl. Fusion 55 (2) (2015) 023013.
[15] H.P. Summers, 2004. The ADAS User Manual version 2.6 . http://adas.phys.strath.ac.uk.
[16] C. Björkas, et al., J. Nucl. Mater. 438 (2013) S276–S279.
[17] A. Pospieszczyk, et al., J. Phys. B 43 (2010) 144017.
[18] A. Kirschener, et al., Nucl. Fus. 40 (2000) 989.